37. ROCK- AND PALEOMAGNETISM OF LEG 43 BASALTS

N. Petersen, Institut für Allgemeine und Angewandte Geophysik, Ludwig-Maximilians Universität, München, West Germany
U. Bleil, Institut für Geophysik, Ruhr-Universität, Bochum, West Germany
and
P. Eisenach, Institut für Allgemeine und Angewandte Geologie, Ludwig-Maximilians Universität, München, West Germany

INTRODUCTION

Ten samples of basalt from Hole 384, four from Hole 386, and six from Hole 387 were analyzed for paleomagnetic and rock magnetic properties. The measurements were complemented by ore microscopic observation. The cored rocks are oriented only with respect to vertical, and so only the inclination of remanent magnetization can be given in absolute values.

MAGNETIC MEASUREMENTS

Methods

Remanent magnetization of the rocks was measured with a Digico spinner magnetometer. Stepwise alternating field demagnetization at 25, 50, 75, 100, 150, 200, 300, 400, 500, and 1000 Oe was carried out in order to determine the stable direction of magnetization.

Volume susceptibility was measured with a Bison magnetic susceptibility bridge. From these values the Koenigsberger Q-ratio (natural remanent magnetization [NRM] $\times$ induced magnetization [$\chi \cdot H$], where χ is the susceptibility and H the earth's magnetic field) was determined. The isothermal saturation remanent magnetization (J_{sr}) was produced in a 10^4 Oe magnetic d.c. field. The coercivity (H_c) was determined by measuring the hysteresis loop (maximum field 10^4 Oe); the coercivity of remanence (H_{cr}) was determined by stepwise reduction of the saturation remanence in magnetic d.c. fields applied in opposite directions.

The Curie temperature (T_c) was determined by measurement of the temperature dependence of the strong-field specific magnetization $I^{1800\ \mathrm{Oe}}$ with a magnetic balance (measured in air at an applied field strength of 1800 Oe). The specific magnetization $I^{1800\ \mathrm{Oe}}$ is measured as magnetic moment per unit weight. If compared with J (measured as magnetic moment per volume), it must be multiplied by the density of the rock.

Results

The results of the magnetic measurements are summarized in Tables 1, 2, and 3. Figures 1(A,B), 2, and 3 show typical thermomagnetic curves.

All samples show relatively high Curie temperatures, mostly higher than 400°C. In comparison, the mean Curie temperature of unaltered Leg 37 basalts is 119°C (Bleil and Petersen, 1977). This difference can most reasonably be explained by subsequent alteration of the magnetic minerals; that is, high- or low-temperature oxidation, or a superposition of both. With the exception of Samples 384-22-CC, 9-11 cm, and 384-22-CC, 46-48 cm, the thermomagnetic curves of all other samples are distinctly irreversible, as is typical when the low-temperature oxidation product maghemite is present. Figure 1(B) illustrates this phenomenon most clearly.

The ratio of saturation remanent magnetization (J_{sr}) and strong field magnetization ($I^{1800\ \mathrm{Oe}}{}_{20°\mathrm{C}}$ $\times$ density of the rock) does not exceed 0.2 and has a mean value of 0.1. As the strong-field magnetization measured in 1800 Oe at room temperature is in first order approximation to the saturation magnetization, these low values suggest multidomain particles to be the dominant carrier of the remanent magnetization. In this context, it is interesting to note the relatively large grain sizes of the titanomagnetites (see Tables 4, 5, 6).

ORE MICROSCOPIC INVESTIGATION

Method

Polished sections of the samples were examined under the ore microscope using a Leitz Ortholux Pol microscope. Magnetic colloid was used as an aid in the identification of the magnetic minerals.

Results

Site 384

A brief description of each sample is given in Table 7. All samples are amygdaloidal phyric basalt in different states of alteration.

Samples 22-1, 118-120 cm (Figures 4 and 5), 22-2, 14-16 cm; and 22-2, 35-37 cm (Figures 6 and 7) are dark gray basalt with abundant subrounded vesicles generally filled with green chlorite. The large skeletal to anhedral titanomagnetites show ilmenite exsolution lamellae and, less commonly, small hematite bodies (deuteric oxidation class 4). Partial maghematization indicates additional subsequent low temperature oxidation (see Figures 4 and 5). There is a remarkable amount of isolated primary ilmenite, which may be as abundant as or more abundant than titanomagnetite.

Samples 22-2, 56-58 cm, and 22-2, 64-66 cm are of a slightly red-brown basalt. They seem to form a transition zone with more elliptical amygdules and veinlets of iron hydroxide. The oxidation state of the opaque minerals and the content of disseminated hematite exceeds that of the overlying basalt.

Samples 22-2, 80-82 cm; 22-2, 106-108 cm; and 22-2, 127-129 cm are red-brown, with calcite-filled amygdules. The oxidation of titanomagnetite has proceeded over ilmenite exsolution lamellae and hematite to iron hydroxide. Even ilmenite is commonly replaced by iron hydroxide. Red staining of the silicate groundmass around the opaque minerals indicates the high oxidation state of these samples.

TABLE 1
Magnetic Parameters of Site 384 Basalts

Sample (Interval in cm)	NRM Intensity (10^{-3} Gauss)	Incl. (°)	Stable Incl. (°)	Susceptibility (10^{-3} Gauss/oe)	Q	MDF (oe)	H_c (oe)	H_{cr} (oe)	J_{sr} (Gauss)	T_c (°C)	$I_{20°C}^{1800\text{ oe}}$ (Gauss·cm^3/g)
22-1, 118-120	2.927	17.5	76.6	1.650	3.23	58	88	160	0.238	340? 585	0.675
22-2, 14-16	1.577	28.4	76.9	1.820	1.58	68	80	148	0.234	555	0.43
22-2, 35-37	1.143	73.3	69.4	1.214	1.71	251	212	360	0.374	550	0.52
22-2, 56-58	0.464	40.2	48.5	0.752	1.12	434	308	412	0.249	575	0.483
22-2, 64-66	0.402	40.1	52.9	0.821	0.89	465	228	520	0.180	550	0.35
22-2, 80-82	6.102	35.0	59.3	2.346	4.73	204	140	292	0.390	600	0.30
22-2, 106-108	2.434	51.2	58.8	1.975	2.24	195	120	264	0.233	385? 580	0.770
22-2, 127-129	1.670	61.7	60.4	1.705	1.78	208	112	256	0.202	600	0.55
22, CC, 104-111	0.882	-34.2	-35.0	0.533	3.01	>1000	>600	–	0.503	180/600	0.359
22, CC, 146-148	4.096	-43.8	-38.7	1.309	5.69	463	240	460	0.305	550	0.540
Mean Values Standard Deviation	2.169 ±1.800	–	pos. incl 62.8 ±10.5 neg. incl -36.8 ±2.6	1.413 ±0.587	2.6 ±1.6	–	–	–	0.290 ±0.102	–	0.558 ±0.177

TABLE 2
Magnetic Parameters of Site 386 Basalts

Sample	NRM Intensity (10^{-3} Gauss)	Incl. (°)	Stable Incl. (°)	Susceptibility (10^{-3} Gauss/oe)	Q	MDF (oe)	H_c (oe)	H_{cr} (oe)	J_{sr} (Gauss)	T_c (°C)	$I_{20°C}^{1800\text{oe}}$ (Gauss·cm^3/g)
66-1 (1)	3.936	37.6	49.1	2.239	3.20	95	84	172	0.217	360	0.60
66-2 (14)	0.643	54.8	60.8	0.513	2.28	122	76	176	0.042	390? 490	0.113
66-2 (21)	2.9 10^{-6}	62.4	62.8	0.056	0.09	197	–	–	1.16 10^{-3}	–	0.013
66, CC (3)	3.590	-66.5	-55.6	3.103	2.10	51	48	100	0.245	345	0.872
Mean Values Standard Deviation	2.043 ±2.008	–	57.1 ±6.2	1.478 ±1.434	1.9 ±1.3	116 ±61	–	–	0.126 ±0.123	372 ±34	0.399 ±0.407

TABLE 3
Magnetic Parameters of Site 387 Basalts

Sample (Interval in cm)	NRM Intensity (10^{-3} Gauss)	Incl. (°)	Stable Incl. (°)	Susceptibility (10^{-3} Gauss/oe)	Q	MDF (oe)	H_c (oe)	H_{cr} (oe)	J_{sr} (Gauss)	T_c (°C)	$I_{20°C}^{1800\text{oe}}$ (Gauss·cm^3/g)
50-1, 22-25	1.347	33.5	48.8	4.512	0.54	50	36	84	0.240	380	1.10
50-1, 35-38	0.949	38.6	53.3	4.390	0.39	39	32	92	0.172	370	1.05
50-1, 98-101	3.237	60.2	67.0	3.321	1.77	101	68	132	0.314	420	0.955
50-2, 30-33	4.050	-52.2?	-58.0?	3.737	1.97	105	76	148	0.349	380	0.90
50-2, 48-51	4.188	66.4	66.3	2.821	2.70	147	92	184	0.352	340	0.77
50-2, 134-137	2.624	-61.5?	-59.2?	3.858	1.24	80	60	124	0.295	370	1.30
Mean Values Standard Deviation	2.733 ±1.358	–	58.8 ±7.1	3.733 ±0.640	1.4 ±0.9	87 ±40	60 ±23	127 ±37	0.287 ±0.070	385 ±79	0.946 ±0.118

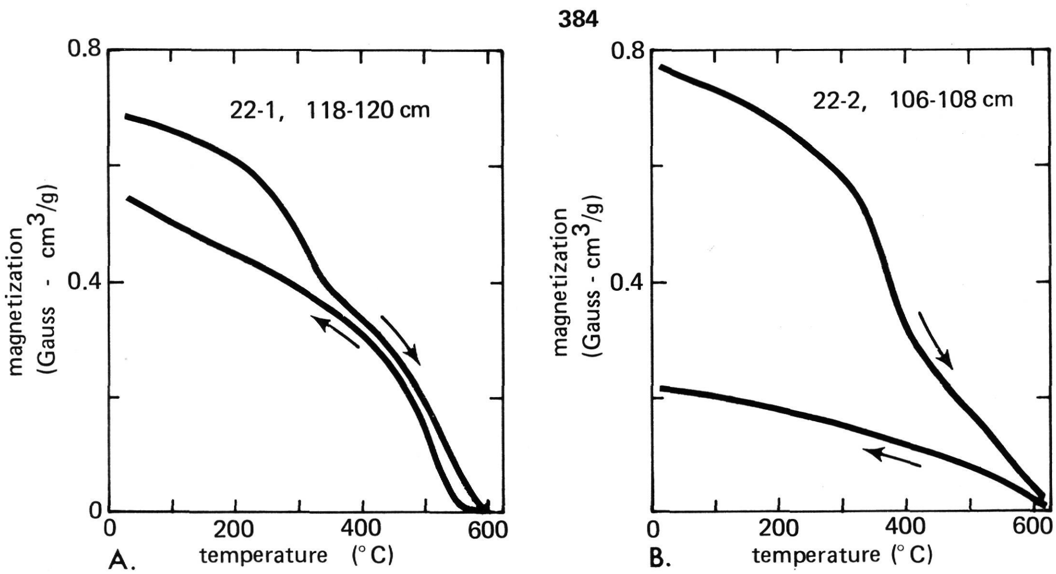

Figure 1. (A and B) *Thermomagnetic curves, measured in air (magnetic field 1800 oe). The irreversibility of heating and cooling curves is indicative of maghemite as main carrier of magnetization.*

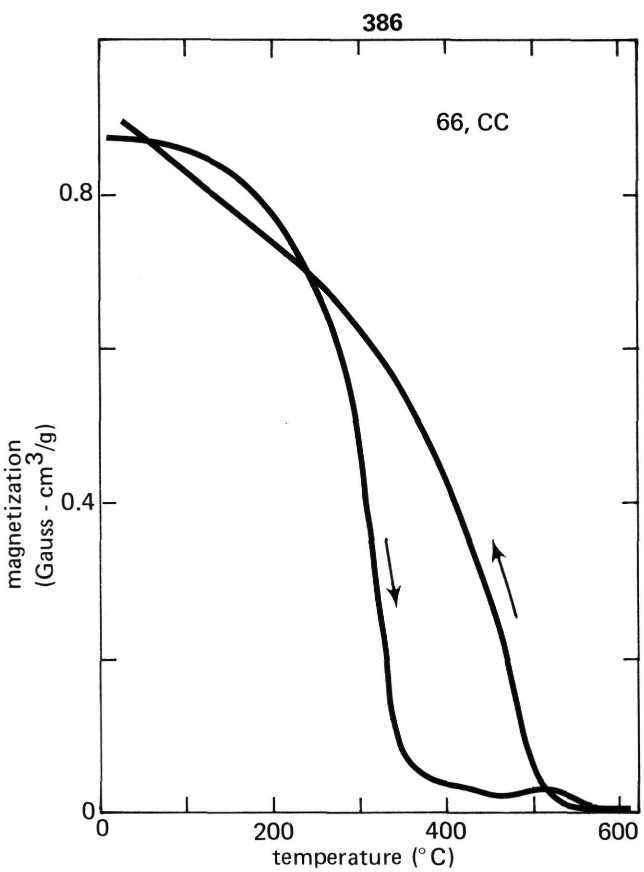

Figure 2. *Thermomagnetic curve, measured in air (magnetic field 1800 oe).*

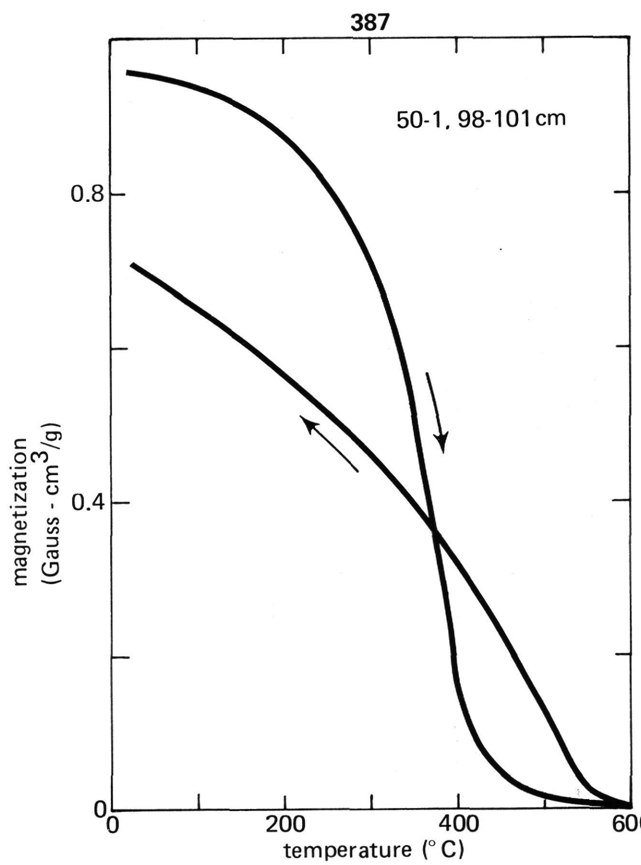

Figure 3. *Thermomagnetic curve, measured in air (magnetic field 1800 oe).*

Basalts of samples 22-CC, 9-11 cm; and 22-CC, 46-48 cm are less altered than the above.

Sulfides are rare in all investigated samples from Site 384. The superposition of deuteric high-temperature oxidation and low-temperature oxidation suggests a complicated thermal history. The large-sized chromites may have formed before eruption under low oxygen pressure.

TABLE 4
Mean Grain Diameter in Microns of the Different Ore Phases in the Site 384 Basalts

Sample (Interval in cm)	Titanomagnetite	Ilmenite	Chromite
22-1, 118-120	31	27	105
22-2, 14-16	20	20	35
22-2, 35-37	35	30	100
22-2, 56-58	45	30	45
22-2, 64-66	30	20	30
22-2, 80-82	15	10	90
22-2, 106-108	30	20	–
22-2, 127-129	20	20	105
22-CC, 109-111	25	15	25
22-CC, 146-148	40	40	–

TABLE 5
Mean Grain Diameter in Microns of the Different Ore Phases in the Site 386 Basalts

Sample	Titanomagnetite	Ilmenite	Chromite
66-2 (14)	<5	–	–
66-2 (21)	<5	–	–
66, CC (3)	30	–	–

TABLE 6
Mean Grain Diameter in Microns of the Different Ore Phases in the Site 387 Basalts

Sample (Interval in cm)	Titanomagnetite	Ilmenite	Chromite
50-1, 22-25	20	–	–
50-1, 35-38	10	–	–
50-1, 98-101	10	–	–
50-2, 30-33	5	–	–
50-2, 134-137	20	–	–

The deuteric high-temperature oxidation (oxidation class 3) may be an indication of crystallization under subaerial or shallow-water conditions. Similar observations have been made for Leg 38 basalts (Norwegian Sea) from Sites 336, 338, and 342 by Kent and Opdyke (1976), and for Leg 26 basalts (Ninety east Ridge) from Sites 253 and 254 by Ade-Hall (1974).

Site 386

A brief description of each individual sample is given in Table 8. Samples 66-23 (4) and 66-2 (21) are material from a hydrothermal vein that cuts the moderately chloritized basalt. The opaque phase of extremely fine grain size is typical for these rocks. Ore phases are too small to be analyzed more closely.

Sample 66, CC (3) is a coarser grained phyric basalt with ophitic texture. The small skeletal grains of titanomagnetite seem to be quite homogeneous and little altered.

Site 387

A brief description of each individual sample is given in Table 9. All samples are fine-grained amygdaloidal phyric basalt with skeletal to anhedral titanomagnetite grains. The titanomagnetites seem to be fairly unaltered which is in contradiction to the thermomagnetic curves. Ilmenite and chromite are absent.

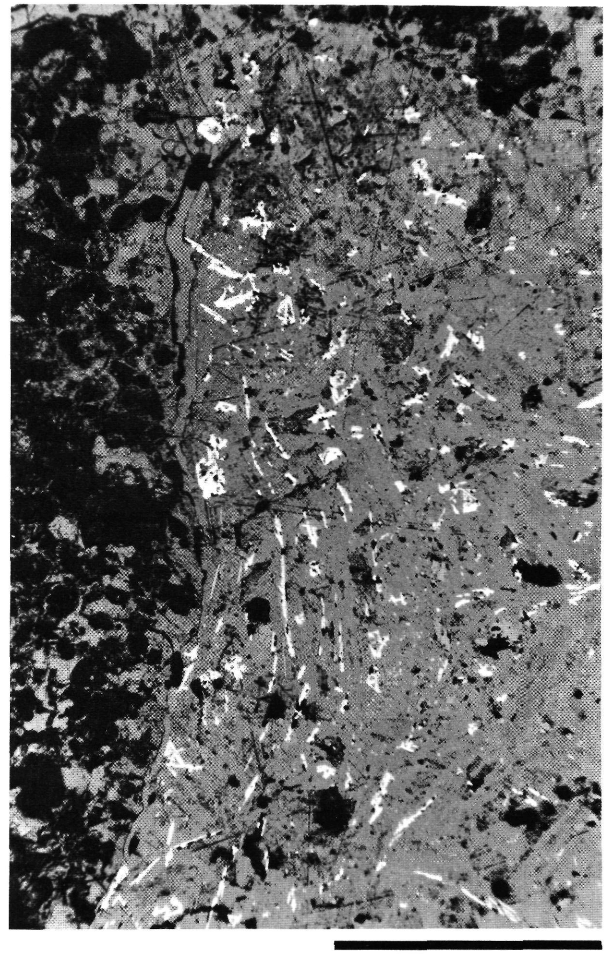

Figure 4. *Fine grained amygdaloidal basalt showing minor fluction of plagioclase and ilmenite around the amygdules. Sample 22-1, 118-120 cm.*

SUMMARY AND DISCUSSION

The carriers of remanent magnetization in the investigated samples are grains of titanomagnetite. There may also be some negligible contribution from sulfides and chromites.

Site 384

High-temperature deuteric oxidation of the titanomagnetites is overprinted by later low-temperature oxidation. Low-temperature oxidation of titanomagnetites is typical for deep ocean weathering (halmyrolysis). In contrast to subaerial basalts, high-temperature oxidation of titanomagnetites seems to be rare in ocean-floor basalts (Ade-Hall et al., 1976) and may only occur in the center of massive flows (Watkins and Haggerty, 1967; Grommé et al., 1969).

Two distinctly different groups of stable magnetization inclination directions were observed: relatively

TABLE 7
Ore Microscopic Description of Site 384 Basalts

Sample (Interval in cm)	General Petrography	Ore Phases: Titanomagnetite	Ilmenite	Chromite	Other Phases
22-1, 118-120	Fine-grained amygdaloidal phyric basalt with varying texture, often showing minor fluxion of plagioclase- and ilmenite laths around the amygdules; commonly ore phase is more abundant in higher reflecting rims around amygdules; basalt is quite vesicular (Fig. 1 and 2)	Skeletal to anhedral grains, from relatively large size down to the limit of visibility; sometimes rimmed by hematite, sometimes mottled, with oxidation to titanomaghemite?	Abundant isolated laths; most grains show signs of oxidation; grains sometimes mantled by titanomagnetite	Large euhedral grains, either homogeneous or with a dark Al-rich core and an outer Fe-rich lighter and often porous zone	Fine-grained hematite fringes around titanomagnetite; rare extremely fine grains of sulfide
22-2, 14-16	Amygdaloidal phyric basalt with rare phenocrysts; quite vesicular (Fig. 3)	Skeletal to anhedral, sometimes with patches of titanomaghemite; grains sometimes contain ilmenite lamellae, not always in definite crystallographic directions (deuteric oxidation?); fringes of fine-grained hematite	Abundant primary ilmenite, mostly with signs of oxidation; slight red staining of groundmass adjacent to ilmenite; ilmenite more abundant than titanomagnetite	Large euhedral to anhedral grains, homogeneous or mottled and porous	Extremely small hematite grains
22-2, 35-37	Amygdaloidal phyric basalt similar to 22-1, 118-120 cm, but no rims of higher reflectivity around amygdules (Fig. 4a and b)	Two generations, large skeletal to anhedral grains and small skeletal grains; the former are altered with patches of titanomaghemite and lamellae of ilmenite; hematite fills cracks and forms fringes, often replaced by iron hydroxide; red staining of the adjacent silicates; smaller generation ti.mag. looks homogeneous without signs of oxidation	Abundant isolated subhedral laths, altered with patches of magnetite	Large euhedral to anhedral grains, sometimes intergrown with skeletal ti.mag; mottled and porous	Iron hydroxides
22-2, 56-58	Altered amygdaloidal phyric basalt; amygdules are lined by a broad seam of iron hydroxide	Highly altered skeletal to anhedral grains with ilmenite lamellae (deuteric oxidation?) and disseminated hematite or iron hydroxide; some grains completely replaced by iron hydroxide; red staining of groundmass around ore grains	Altered isolated laths, partly with patches of magnetite	Few large euhedral grains with dark core	Abundant iron hydroxide in the amygdules and also partly replacing titanomagnetite
22-2, 64-66	Amygdaloidal phyric basalt with increasing content of calcite	Altered skeletal to anhedral grains containing ilmenite lamellae (deuteric oxidation?) red staining of adjacent silicates; some grains replaced by iron hydroxide	Isolated laths, marginally oxidized to magnetite	Like 22-1, 118-120 cm; more frequent adjacent to amygdules	Iron hydroxide
22-2, 80-82	Amygdaloidal phyric basalt similar to 22-1, 118-120 cm; red staining of groundmass close to opaque minerals	Highly altered small skeletal grains, partly with ilmenite-magnetite exsolution (deuteric oxidation) magnetite often being replaced by hematite; sometimes replaced by iron hydroxide	Less and small isolated laths, highly altered, disseminated by hematite and iron hydroxide	Large euhedral grains with rims of magnetite, partly replaced by iron hydroxide	Abundant iron hydroxide
22-2, 106-108	Amygdaloidal phyric basalt with texture similar to 22-1, 118-120 cm; red staining of groundmass around Fe-Ti oxides	Small skeletal to anhedral grains, highly altered; exsolved ilmenite lamellae replaced by iron hydroxide; spinel exsolution	Rare, highly altered isolated laths, marginally replaced by iron hydroxide	Euhedral to anhedral grains, some mottled and porous, some homogeneous	Abundant iron hydroxide
22-2, 127-129	Amygdaloidal phyric basalt with calcite veins; red staining of silicate groundmass around opaque minerals	Like 22-2, 106-108 cm	Similar to 22-2, 106-108 cm, but slightly less oxidized	Euhedral to anhedral grains, sometimes mantled by titanomagnetite containing secondary exsolution lamellae	Abundant iron hydroxide
22-CC, 109-111	Amygdaloidal phyric basalt; red staining of groundmass around opaque minerals	Small skeletal grains with ilmenite exsolution lamellae (deuteric oxidation?) and very fine disseminated hematite	Small isolated laths, sometimes with signs of oxidation	Large subhedral grains, mottled and porous	Not observed
22-CC, 146-148	Amygdaloidal phyric basalt with ophitic texture	Skeletal grains with ilmenite exsolution lamellae and very fine disseminated hematite; sometimes corroded with red staining of adjacent silicate groundmass	Homogeneous laths, sometimes mantled by titanomagnetite; beginning oxidation with veinlets of hematite on the limit of visibility	Subhedral to anhedral grains, mottled and porous	Iron hydroxides and extremely fine grains of sulfides

Figure 5. *Skeletal titanomagnetite and large ilmenite laths. Sample 22-1, 118-120 cm.*

Figure 6. *Large anhedral chromite pseudomorph to titanomagnetite (snowstar). Mottled dark gray porous core and a rim of titanomagnetite. Sample 22-2, 14-16 cm.*

steep (mean 62.8°) for the upper samples, and shallow (mean –36.8°) for the two lowermost samples.

The present magnetic dipole field inclination at the latitude of Site 384 is 59.5°. If we assume a Cretaceous date for the measured basalts, the inclination to be expected at Site 384 is 41.8° (taking a Cretaceous pole position for the North American plate of 64°N, 173°W; McElhinny, 1973). Comparing this inclination with the measured magnetization inclinations, we find reasonable agreement only for the shallow inclinations of the two lower samples. The steep inclination of the upper samples compares much better with the present geomagnetic dipole field of 59.5°.

Taking into account the rock magnetic data, we conclude that only the two lower samples, 22-CC, 109-111 cm, and 22-CC, 146-148 cm, have retained their original thermoremanent magnetization. The other samples most likely have lost their primary magnetization owing to low-temperature oxidation of the magnetic minerals; the present remanent magnetization of these

TABLE 8
Ore Microscopic Description of Site 386 Basalts

Sample (Interval in cm)	General Petrography	Ore Phases: Titanomagnetite	Ore Phases: Ilmenite	Ore Phases: Chromite	Ore Phases: Other Phases
66-2 (14)	–	Extremely fine grained; too fine for further microscopic identification	Extremely fine grained	Not observed	
66-2 (21)	–	Like 66-2 (14)	Like 66-2 (14)	Not observed	Small sulfide grains
66, CC (3)	Coarser grained phyric basalt with bulky texture of the plagioclase laths	Small skeletal grains which look homogeneous and unaltered; sometimes intergrown with sulfides	Abundant isolated unaltered laths	Not observed	Sulfides of varying grain size down to the limit of visibility, partly intergrowth of pyrite and bornite

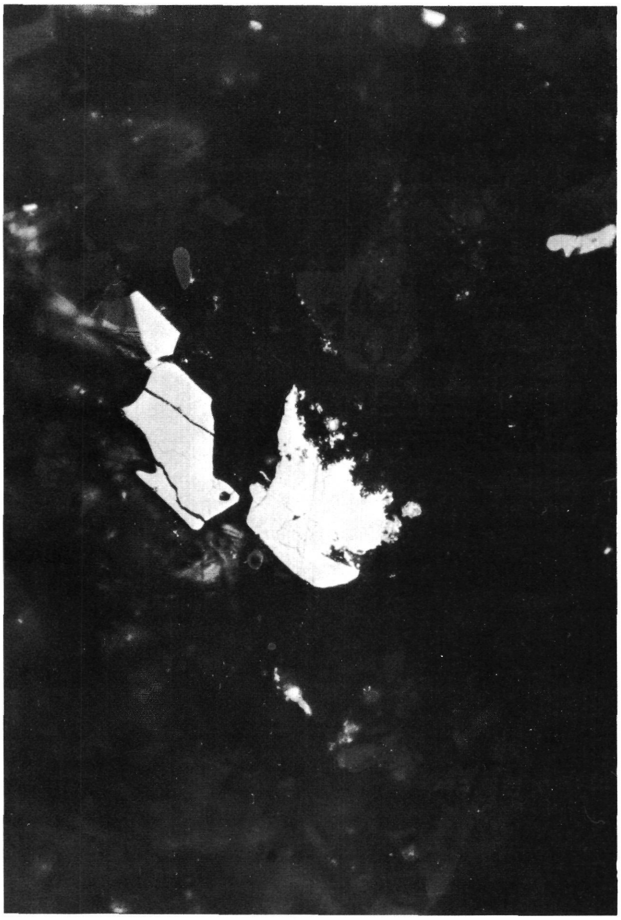

Figure 7a. *Homogeneous titanomagnetite without sign of oxidation. Sample 22-2, 35-38 cm.*

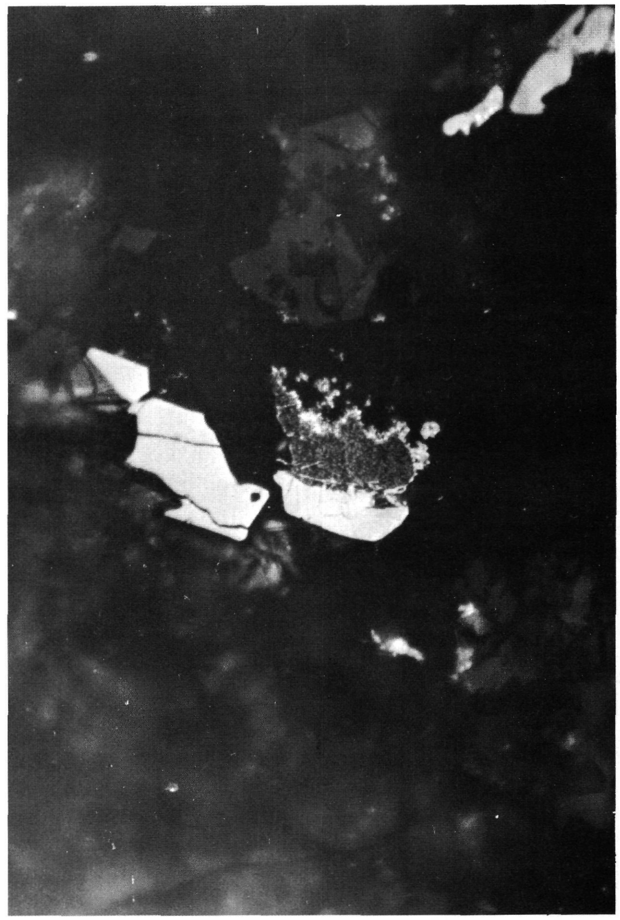

Figure 7b. *The same grain with magnetic colloid shows a sharp separation in a magnetic and nonmagnetic part. This fact is a consequence of maghemitization.*

TABLE 9
Ore Microscopic Description of Site 387 Basalts

Sample (Interval in cm)	General Petrography	Ore Phases			Other Phases
		Titanomagnetite	Ilmenite	Chromite	
50-1, 22-25	Coarser grained phyric basalt with abundant plagioclase phenocrysts; ophitic texture	Large skeletal and small anhedral to subhedral grains; large grains; large grains are fringed by a fine second generation; most grains with volume change cracks, but no other indication of oxidation	Not observed	Not observed	Small sulfide grains
50-1, 35-38	Fine-grained amygdaloidal phyric basalt with bulky texture of plagioclase laths; slightly fewer phenocrysts than in 50-1, 22-25 cm	Anhedral to subhedral grains from relatively large down to the limit of visibility; larger grains show cracks with volume change, and small fringes of extremely fine grained second generation	Not observed	Rare large euhedral grains with rims of titanomagnetite	Small sulfide grains
50-1, 98-101	Fine-grained phyric basalt with large plagioclase phenocrysts; ophitic texture	Extremely small skeletal grains	Not observed	Not observed	Small sulfide grains
50-2, 30-33	Fine-grained amygdaloidal phyric basalt with varying texture	Extremely fine anhedral to skeletal grains	Not observed	Not observed	Tiny sulfide grains
50-2, 134-137	Coarser grained amygdaloidal phyric basalt with ophitic texture	Small skeletal grains sometimes bordered by sulfide grains	Rare small isolated laths	Not observed	Small sulfide grains

rocks appears to be a chemical remanence acquired at some time after the emplacement of the rock. In this context, it is interesting to note that during the Tertiary the paleomagnetic pole of the North American plate was very close to the present North Pole.

Site 386

The samples show low-temperature oxidation of the titanomagnetites. At Site 368 the measured magnetization inclination values (mean 57.1°) are also much steeper than the expected inclination of 36.3° for the Cretaceous. The present dipole field inclination of 50.4° compares better with the measured values, which again suggests the buildup of a later chemical magnetization due to alteration of the magnetic minerals.

For Sample 66, CC (3), however, rock magnetic data do not support this conclusion as clearly as for the other samples.

Site 387

The situation here is more or less the same as in previous cases. The magnetic titanomagnetites have been altered by low-temperature oxidation.

The expected Cretaceous field inclination at Site 387 of 39.6° is much shallower than the measured inclinations (mean 58.8°), which is close to the present magnetic dipole field inclination (51.7°).

In agreement with the rock magnetic data, the measured magnetization is also interpreted as a chemical remanent magnetization that has been built up over an extended period long after initial emplacement of the rocks. The original thermoremanent magnetization of the rocks has most likely been destroyed by low-temperature oxidation of the titanomagnetites.

ACKNOWLEDGMENTS

This study is a combined contribution of the Institut für Allgemeine und Angewandte Geophysik, of the Institut für Allgemeine und Angewandte Geologie, both Ludwig-Maximilians Universität, München, and of the Institut fur Geophysik, Ruhr-Universität, Bochum. We thank Prof. Dr. G. Angenheister, Prof. Dr. D. Klemm, and Prof. Dr. H. Baule for generously making available the facilities of the above named institutions and for their support throughout the study. The manuscript was reviewed by D. Kent and P. Vogt. The financial support of the Deutsche Forschungsgemeinschaft is gratefully acknowledged.

REFERENCES

Ade-Hall, J. M., 1974. Strong field magnetic properties of basalts from DSDP Leg 26. *In* Davies, T. A., Luyendyk, B., et al., *Initial Reports of the Deep Sea Drilling Project,* v. 26: Washington (U.S. Government Printing Office), p. 529-532.

Ade-Hall, J. M., Fink, L. K., and Johnson, H. P., 1976. Petrography of opaque minerals, Leg 34. *In* Hart, J. R., Yeats, R. S., et al., *Initial Reports of the Deep Sea Drilling Project,* v. 34: Washington (U.S. Government Printing Office), p. 349-362.

Bleil, U. and Petersen, N., 1977. Magnetic properties of basement rocks, Leg 37, Site 332. *In* Aumento, F., Melson, W. G., et al., *Initial Reports of the Deep Sea Drilling Project,* v. 37: Washington (U.S. Government Printing Office), p. 446-456.

Grommé, C. S., Wright, T. L., and Peck, D. L., 1969. Magnetic properties and oxidation of iron-titanium oxide minerals in Alae and Makaopuhi lava lakes, Hawaii: *J. Geophys. Res.*, v. 74, p. 5277-5293.

Kent, D. V. and Opdyke, N. D., 1976. Paleomagnetism and magnetic properties of igneous rock samples—Leg 38. *In* Talwani, M., Udintsev, G., et al., *Initial Reports of the Deep Sea Drilling Project*, Supplement to Volumes 38, 39, 40, and 41: Washington (U.S. Government Printing Office), p. 3-8.

McElhinny, M. W., 1973. Paleomagnetism and plate tectonics. Cambridge (Cambridge University Press).

Watkins, N. D. and Haggerty, S. E., 1967. Primary oxidation variation and petrogenesis in a single lava: *Contrib. Mineral. Petrol.,* v. 15, p. 251-271.